Prediction-Based Compression Ratio Boundaries for Medical Images

Xiaojun Qi
Computer Science Department, Utah State University
4205 Old Main Hill, Logan, UT 84322
Xiaojun.Qi@usu.edu

Abstract

Most present prediction-based image compression techniques take advantage of either intra- or inter-image correlation or both to de-correlate images. These de-correlated images usually contain reduced information content. Consequently, higher compression ratios may be obtained from these de-correlated images. This paper studies the relationship between image correlation and the resultant information redundancy, and develops a method for estimating the compression ratio C, which is a function of the image correlation ρ. The compression boundaries (i.e., the maximum compression ratios) are further derived from this compression ratio function. The prediction-based compression technique has been applied on some magnetic resonance (MR) brain image sets to numerically prove the derived compression boundaries.

1. Introduction

Prediction-based image compression techniques [1-7] have been widely used in lossless coding schemes. These techniques include linear and adaptive nonlinear predictions. The differentiation-based linear prediction technique has also been adopted for lossless compression in the JPEG still picture compression standard [1]. In general, the prediction-based image compression technique estimates each predicted pixel value from the appropriately weighted neighboring pixel values from either the currently predicted image or the previously encoded image in an image sequence. That is, the intensity of each pixel is predicted according to a weighted sum of its causal neighbors and rounded to the nearest integer value:

$$g'(x,y,k) = INT\left(\sum_{i=0}^{2}\sum_{j=-1}^{2}\sum_{k=0}^{1} a(i,j,k)g(x-i,y-j,z-k)\right) \quad (1)$$

where:

- The *i*'s, *j*'s, and *k*'s respectively are the distances from a causal neighboring pixel to the predicted pixel along *x, y,* and *z* directions, where *x* is the vertical direction of the image starting from the top left corner and going downwards, *y* is the horizontal direction of the image, and *z* is the image axis direction starting from the first to the last image in an image set;
- The $a(i,j,k)$'s are the predictor coefficients (i.e., causal neighbors' weights);
- The $g(x-i,y-j,z-k)$ and $g'(x,y,k)$ are the gray-level intensities of the causal neighboring pixel and the predicted pixel at the coordinates of $(x-i,y-j,z-k)$ and (x,y,z), respectively.

The prediction residual (i.e., error) $e(x,y,z)$ is calculated by subtracting each estimated pixel value from the corresponding original pixel value in an image sequence:

$$e(x,y,z) = g(x,y,z) - g'(x,y,z) \quad (2)$$

where *x*'s, *y*'s, and *z*'s range from the minimum to the maximum value in each of the three directions (i.e., horizontal, vertical, and axis directions). This prediction residual is stored instead of the original.

The original image can be completely recovered from the prediction coefficients (i.e., $a(i,j,k)'s$) and the prediction residuals (i.e., $e(x,y,z)'s$). Therefore, if the prediction model precisely estimates most pixel intensities (i.e., $g(x,y,z)'s$) in the original image, the residual distribution can be closely approximated by a Laplace distribution curve where most residuals are small and are thus concentrated at the top of the residual distribution curve. Such distribution tends to have less information and be easier to compress by any conventional encoding technique. That is, prediction-based compression technique produces its best compression when neighboring pixels in an image or neighboring images in an image sequence are similar (i.e., have comparable pixel intensity and are highly correlated to each other). Therefore, the compression ratios yielded by the prediction-based technique are proportional to the correlation $\rho = Corr(u,u')$ between the original image u and its projection u' onto the predictor set. This projection image is represented by $g(x-i,y-j,z-k)$ in the equation (1). Correspondingly, the compression ratio can be estimated as:

$$C(\rho) = \frac{H(u)}{H(r)} = \frac{H(u)}{H(u-u')} = \frac{1}{HR(\rho)} \quad (3)$$

where $H(\ )$ is Shannon entropy [8], and $HR(\rho)$ is the entropy reduction function which measures the relative amount of information in u which can not be linearly predicted from u'.

This paper analytically determines compression ratio boundaries for the prediction-based techniques in terms of the dependencies between ρ and $C(\rho)$. The compression results from the prediction-based techniques are demonstrated on medical image sets containing multiple single images. These numerical examples prove our analytical results.

2. Compression Ratio Boundaries

Given an n gray-scale image u (original image) and its projection image v, the compression ratio can be estimated as:

$$C(\rho) = \frac{H(u)}{H(u-v)} = \frac{1}{HR(\rho)} \tag{4}$$

where $\rho = Corr(u,v)$ represents the correlation between u and v, and $HR(\rho)$ is a function of a probability distribution:

$$P = \left\{P_{ij} = P(u = i \text{ and } v = j)_{0 \le i,j \le n-1}\right\} \tag{5}$$

Therefore, the maximum and minimum information reduction over all ρ-correlated n gray-scale original and projection image pairs are:

$$\begin{aligned} HR^{\max}(n,\rho) &= \max_{P:\rho(u,v)=\rho} HR(n,\rho), \\ HR^{\min}(n,\rho) &= \min_{P:\rho(u,v)=\rho} HR(n,\rho) \end{aligned} \tag{6}$$

The corresponding minimum and maximum compression ratios are:

$$\begin{aligned} C^{\min}(n,\rho) &= \frac{1}{HR^{\max}(n,\rho)}, \\ C^{\max}(n,\rho) &= \frac{1}{HR^{\min}(n,\rho)} \end{aligned} \tag{7}$$

Similarly, given a sequence of images with the correlation ranging from ρ_1 to ρ_2 between any original and projection image pair, the average minimum and maximum compression ratios can be estimated as:

$$\begin{aligned} C^{\min}(n,[\rho_1,\rho_2]) &= \frac{1}{\rho_2-\rho_1}\int_{\rho=\rho_1}^{\rho_2} C^{\min}(n,\rho)d\rho \\ C^{\max}(n,[\rho_1,\rho_2]) &= \frac{1}{\rho_2-\rho_1}\int_{\rho=\rho_1}^{\rho_2} C^{\max}(n,\rho)d\rho \end{aligned} \tag{8}$$

The dependencies between ρ and $C(\rho)$ can be easily derived for binary images. The intensity probability for any binary image u and its projection binary image v is:

$$P = \left\{P_{ij} = P(u = i \text{ and } v = j)_{0 \le i,j \le 1}\right\} \tag{9}$$

where:

$$\begin{aligned} &p_1 = P(u=0 \text{ and } v=0);\ p_2 = P(u=1 \text{ and } v=0); \\ &p_3 = P(u=0 \text{ and } v=1);\ p_4 = P(u=1 \text{ and } v=1). \end{aligned} \tag{10}$$

The intensity probability for the residual $r = u - v$ is:

$$P_r = \begin{Bmatrix} P(r=-1) = p_3, \\ P(r=0) = p_1 + p_4, \\ P(r=1) = p_2 \end{Bmatrix} \tag{11}$$

The correlation between these two binary images is calculated as:

$$\begin{aligned} Corr(u,v) &= \frac{Cov(u,v)}{\sigma_u\sigma_v} \\ &= \frac{\sum_{i=0}^{1}\sum_{j=0}^{1} P(u=i \text{ and } v=j)(i-\bar{u})(j-\bar{v})}{\sigma_u\sigma_v} \\ &= \frac{\sum_{i=0}^{1}\sum_{j=0}^{1} P(u=i \text{ and } v=j)(i-(p_2+p_4))(j-(p_3+p_4))}{\sqrt{(p_1+p_3)(p_2+p_4)}\sqrt{(p_1+p_2)(p_3+p_4)}} \\ &= \frac{p_1(p_2+p_4)(p_3+p_4) - p_2(1-p_2-p_4)(p_3+p_4)}{\sqrt{(p_1+p_3)(p_2+p_4)}\sqrt{(p_1+p_2)(p_3+p_4)}} \\ &+ \frac{-p_3(p_2+p_4)(1-p_3-p_4) + p_4(1-p_2-p_4)(1-p_3-p_4)}{\sqrt{(p_1+p_3)(p_2+p_4)}\sqrt{(p_1+p_2)(p_3+p_4)}} \\ &= \frac{p_1 - p_1^2 - 2p_1p_2 - p_2^2}{\sqrt{(p_1+p_3)(p_2+p_4)}\sqrt{(p_1+p_2)(p_3+p_4)}} \end{aligned} \tag{12}$$

The following two conditions are taken into account to simplify the derivation:

(1) $\sum_{i=1}^{4} p_i = 1$ and $p_i \ge 0$, which are true for any binary image.

(2) $\sigma^2(u) = \sigma^2(v)$, which can be satisfied by a simple rescaling procedure.

By combining these two conditions, $p_2 = p_3$ can be determined and the equation (12) can be simplified by:

$$\begin{aligned} \rho = Corr(u,v) &= \frac{Cov(u,v)}{\sigma_u\sigma_v} \\ &= \frac{p_1 - p_1^2 - 2p_1p_2 - p_2^2}{p_1 + p_2 - p_1^2 - 2p_1p_2 - p_2^2} \end{aligned} \tag{13}$$

Therefore, the binary intensity probability can be expressed as a function of p_1 and ρ such that:

$$\begin{aligned} p_2 = p_3 &= \frac{-\rho + 2\rho p_1 - 2p_1 + \sqrt{\rho^2 - 4\rho p_1 + 4p_1}}{2(1-\rho)} \\ p_4 &= \frac{1 + p_1 - \rho p_1 - \sqrt{\rho^2 - 4\rho p_1 + 4p_1}}{1-\rho} \end{aligned} \tag{14}$$

These probabilities are substituted into equation (4) so

the compression ratio can be expressed in terms of the probability p_1 and the correlation ρ.

$$C(n=2,\rho,\rho_1)=\frac{H(v)}{H(u-v)}$$
$$=\frac{(p_1+p_3)\log_2(p_1+p_3)+(p_2+p_4)\log_2(p_2+p_4)}{p_2\log_2(p_2)+(p_1+p_4)\log_2(p_1+p_4)+p_3\log_2 p_3} \quad (15)$$

Table I numerically presents the dependencies between C and (ρ, p_1) pairs based on the equation (15). These results are computed by varying the correlation and the probability from 0 to 1 with an increasing step size of 0.02 and 0.05, respectively.

Table I Relationship between C and (ρ, p_1) pairs

ρ	p_1	$C^{\max}$	p_1	$C^{\min}$	ρ	p_1	$C^{\max}$	p_1	$C^{\min}$
.00	.25	**.6667**	.95	.5115	.52	.40	**.9660**	.9	.9153
.02	.25	**.6712**	.95	.5198	.54	.40	**.9920**	.9	.9458
.04	.25	**.6761**	.95	.5283	.56	.40	**1.0202**	.9	.9787
.06	.25	**.6813**	.95	.5372	.58	.40	**1.0510**	.05	1.0144
.08	.25	**.6867**	.95	.5464	.60	.40	**1.0847**	.05	1.0532
.10	.30	**.6926**	.95	.5560	.62	.40	**1.1217**	.85	1.0950
.12	.30	**.6992**	.95	.5644	.64	.95	**1.1627**	.95	1.1373
.14	.30	**.7061**	.95	.5741	.66	.95	**1.2091**	.1	1.1908
.16	.30	**.7135**	.95	.5873	.68	.95	**1.2698**	.5	1.2469
.18	.30	**.7212**	.95	.5986	.70	.95	**1.3379**	.65	1.2945
.20	.30	**.7294**	.95	.6104	.72	.95	**1.4149**	.75	1.3757
.22	.30	**.7381**	.95	.6228	.74	.95	**1.5028**	.7	1.4525
.24	.30	**.7473**	.95	.6358	.76	.95	**1.6040**	.6	1.5396
.26	.30	**.7570**	.95	.6494	.78	.95	**1.7222**	.45	1.6396
.28	.30	**.7674**	.95	.6637	.80	.95	**1.8621**	.45	1.7575
.30	.35	**.7784**	.95	.6787	.82	.95	**2.0306**	.45	1.8994
.32	.35	**.7904**	.95	.6945	.84	.95	**2.2379**	.45	2.0739
.34	.35	**.8031**	.95	.7111	.86	.95	**2.4997**	.65	2.1975
.36	.35	**.8167**	.95	.7236	.88	.95	**2.8418**	.75	2.4575
.38	.35	**.8311**	.95	.7474	.90	.95	**3.3102**	.5	2.9731
.40	.35	**.8465**	.95	.7671	.92	.95	**3.9942**	.65	3.3978
.42	.35	**.8630**	.95	.7881	.94	.95	**5.0976**	.65	4.5980
.44	.35	**.8807**	.95	.8105	.96	.95	**7.2119**	.5	6.1945
.46	.35	**.8996**	.95	.8343	.98	.95	**13.1504**	.5	11.0142
.48	.35	**.9200**	.95	.8598	1.0		∞		∞
.50	.40	**.9420**	.9	.8870					

The results presented on Table I demonstrate that the higher correlation between the original and projection binary images leads to higher compression ratios. If the correlation is inclusively above 0.58, the predication-based techniques achieve compression for any intensity distribution function. Otherwise, there are not any compression gains for any intensity distribution function.

For 8-bit gray-scale images, the intensity probability depends on $n^2=256^2$ (u,v) pairs, where u and v range from 0 to 255. Therefore, the derivation of the compression ratio boundaries for n gray-scale images can be complicate and time-consuming. To simplify the derivation procedure, we extend our binary results to certain gray-scale images (i.e., medical images). This expansion is based on the observation that most medical images contain a dark background and a light foreground. As a result, two distinct intensity clusters representing background and foreground can be determined by an appropriate threshold method. This observation is illustrated with the histogram of an MR brain image shown on Fig 1. After setting every pixel above the threshold determined from the histogram, a binary image representing the original image can be derived.

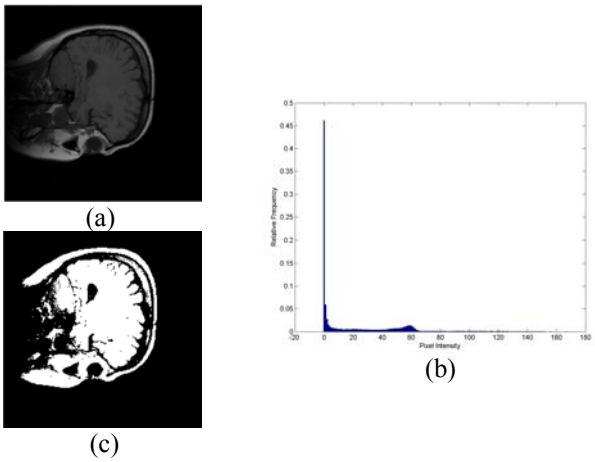

Figure 1: Conversion from gray-scale to binary images (a) Original MR brain image (b) Histogram (c) Thresholded MR brain image (binary image)

Therefore, we expand our results from a binary domain to a gray-scale domain as:

$$C^{\max}(n_1,\rho)\le C^{\max}(n_2,\rho) \qquad \text{if } n_1\ge n_2 \quad (16)$$

That is, if the gray-scale original and projection images have the correlation of 0.58, the maximum compression ratios must be lower than 1.0510. The correlation of 0.82 guarantees a maximum approximated compression ratio of 2:1.

3. Experimental Results

In our research, MR brain image sets obtained from two different sources are used to illustrate the dependencies between the compression ratios and the correlation. The first source is an MRI simulator developed at the McConnell brain imaging center [9]; the second source is Louisiana State University Health Sciences Center in New Orleans (LSUHSC-NO). All simulated and real MR brain image sets were acquired by different cross sections including axial, sagittal, and coronal. They contain 14 to 24 8-bit (256 gray-scale) images.

Three types of predictors (i.e., intra-, intra-and-inter-, and inter-image predictors) have been implemented to demonstrate the relationship between the compression

ratios and the correlations. These three types of predictors respectively use the linear combination of two intra-image pixels (i.e., A and B), one intra-image pixel and one inter-image pixel (i.e., B and C), and two inter-image pixels (i.e., C and D) to estimate pixel intensity at the position of X, as illustrated on Figure 2.

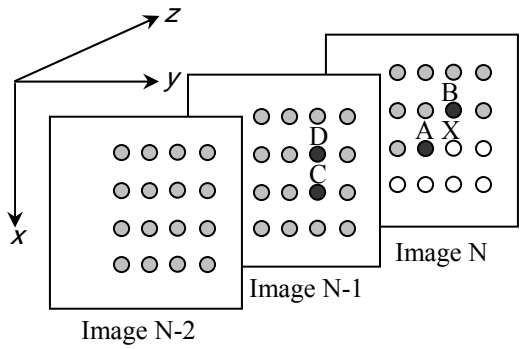

The predicted pixel represented by a white circle:

$$X = g(x, y, z)$$

Causal neighboring pixels represented by dark circles:

$$A = g(x, y-1, z), B = g(x-1, y, z),$$

$$C = g(x, y, z-1), D = g(x-1, y, z-1)$$

Figure 2: Sample prediction neighborhoods

Table II shows the prediction-based compression results of the MR brain image sets from two sources. Arithmetic coding implemented by Moffat [10] is utilized for the entropy coding on the prediction residuals. The results on three rows for each image set are respectively obtained from the intra-, intra-and-inter, and inter-image predictors as illustrated on Figure 2.

Table II Predicted entropy coded compression results

Simulated MR Brain Sets			Real MR Brain Sets		
Set No.	ρ	$C(\rho)$	Set No.	ρ	$C(\rho)$
1	.9776	2.5912	1	.9593	1.9372
	.8918	2.3278		.8418	1.8387
	.8007	1.4959		.7198	1.3905
2	.9617	2.5342	2	.9728	1.8940
	.8267	2.0908		.8456	1.7322
	.6840	1.2404		.7146	1.3347
3	.9851	2.6963	3	.9489	1.5676
	.9194	2.5235		.8126	1.5100
	.8490	1.8820		.6615	1.1929
4	.9629	2.5496	4	.9691	1.9856
	.8280	2.0855		.8600	1.8813
	.6867	1.2441		.7436	1.4721
5	.9861	2.5722	5	.9680	1.7907
	.9113	2.3524		.8467	1.6609
	.8329	1.2750		.7190	1.3087
6	.9617	2.3813	6	.9327	1.5422
	.8177	2.0180		.8093	1.4832
	.6861	1.2314		.6686	1.1998

The results numerically prove the prediction-based compression ratio boundaries shown in Table I. For example, the original and projection images of the second image set from the real MR brain image sets have a correlation of 0.8456. The compression ratio achieved is 1.7322, which is less than the upper bound of 2.2379.

4. Conclusions

A mathematical approach has been presented for evaluating the efficiency of any prediction-based image compression technique. This mathematical approach studies the relationship between the compression ratios and the correlations. The numerical computation produces an approximated estimation of the best achievable compression ratios. These analysis results can be applied to a variety of images.

References

[1] G. K. Wallace, "The JPEG still picture compression standard," *Communication ACM*, Vol. 34, pp. 30-44, 1991.

[2] P. Roos, M. A. Viergever, M. C. A. Van Dijke, and J. H. Peters, "Reversible intraframe compression of medical images," *IEEE Transactions on Medical Imaging*, Vol. 7, No. 4, pp. 328-336, 1992.

[3] M. Das and S. Burgett, "Lossless compression of medical images using two-dimensional multiplicative autoregressive models," *IEEE Transactions on Medical Imaging*, Vol. 12, No. 4, pp. 721-726, 1993.

[4] J. Lee, "Quadtree-based least-squares prediction for multispectral image coding," *Optical Engineering*, Vol. 37, No. 5, pp. 1547-1552, 1998.

[5] T. Nakachi, T. Fujii, and J. Suzuki, "Pel adaptive predictive coding based on image segmentation for lossless compression," *IEICE Transaction Fundamentals*, Vol. E82-A, No. 6, pp. 1037-1046, 1999.

[6] K. Rose, S. L. Regunathan, "Toward optimality in scalable predictive coding," *IEEE Transactions on Image Processing*, Vol. 10, No. 7, pp. 965-976, 2001.

[7] A. Jagmohan, A. Sehgal, and N. Ahuja, "Predictive encoding using coset codes," *Proceedings of International Conference on Image Processing*, Rochester, New York, pp. 29-32, Sept. 2002.

[8] C. E. Shannon, "A mathematical theory of communication," *Bell Systems Technical Journal*, Vol. 27, pp. 379-423, 1948.

[9] http://www.bic.mni.mcgill.ca/brainweb/

[10] A. Moffat, R. Neal, and I. H. Witten, "Arithmetic coding revised," *ACM Transactions on Information Systems*, Vol. 3, 256-294, 1998.